LUND UNIVERSITY

Modeling Analysis of Different Renewable Fuels in an Anode Supported SOFC

Andersson, Martin; Paradis, Hedvig; Yuan, Jinliang; Sundén, Bengt

Link to publication

Paper III

Modeling Analysis of Different Renewable Fuels in an Anode Supported SOFC

Martin Andersson
e-mail: martin.andersson@energy.lth.se

Hedvig Paradis

Jinliang Yuan

Bengt Sundén

Department of Energy Sciences,
Faculty of Engineering,
Lund University,
Box 118,
221 00 Lund, Sweden

It is expected that fuel cells will play a significant role in a future sustainable energy system due to their high energy efficiency and possibility to use as renewable fuels. Fuels, such as biogas, can be produced locally close to the customers. The improvement for fuel cells during the past years has been fast, but the technology is still in the early phases of development; however, the potential is enormous. A computational fluid dynamics (CFD) approach (COMSOL MULTIPHYSICS) is employed to investigate effects of different fuels such as biogas, prereformed methanol, ethanol, and natural gas. The effects of fuel inlet composition and temperature are studied in terms of temperature distribution, molar fraction distribution, and reforming reaction rates within a singe cell for an intermediate temperature solid oxide fuel cell. The developed model is based on the governing equations of heat, mass, and momentum transport, which are solved together with global reforming reaction kinetics. The result shows that the heat generation within the cell depends mainly on the initial fuel composition and the inlet temperature. This means that the choice of internal or external reforming has a significant effect on the operating performance. The anode structure and catalytic characteristic have a major impact on the reforming reaction rates and also on the cell performance. It is concluded that biogas, methanol, and ethanol are suitable fuels in a solid oxide fuel cell system, while more complex fuels need to be externally reformed. [DOI: 10.1115/1.4002618]

Keywords: SOFC, modeling, biogas, methanol, ethanol, natural gas, reforming, COMSOL MULTIPHYSICS

1 Introduction and Problem Statement

Fuel cells (FCs) are promising due to its environmental advantages with higher efficiency and lower emissions of SO_x, NO_x, and CO_2 than conventional power generation [1]. The solid oxide fuel cell (SOFC) works at a high temperature such as $600-1000\,^\circ C$ [2]. This allows SOFCs to operate with different types of fuels from both fossil and renewable sources. It opens up for an easier transition from conventional power generation with hydrocarbon based fuels to fuel cells with possibility for different fuels, especially SOFCs. Due to the increasing global awareness of how energy usage affects the environment, the interest of renewable energy has increased. SOFCs are generally more tolerant to contaminants than other fuel cells and the possibility to internally (as well as externally) reform the fuel makes them interesting for renewable energy resources [1]. Attractive fuels, which are considered in this study, are biogas, methanol, ethanol, and natural gas. The list of potential fuels for SOFC systems also includes gasoline, diesel, aviation fuel, ammonia, acetic acid, formic acid, butanol, butyric acid, and bottled gas. Coal and biomass can be used as raw fuels in a gasification process, which takes place before the fuel cell stack [3].

The aim of this paper is to study the possibility of using renewable fuels in SOFCs. The reforming reactions in SOFC systems can be conducted both externally and internally. The external reforming (ER), such as the prereformer in a SOFC system, means that the reformer is placed outside the cell, which is possible for all types of fuel cells. The internal reforming (IR) means that the reforming reactions occur within the cell. In the direct internal reforming (DIR) approach, the reforming processes occur together with the electrochemical reactions within the anode. In the indirect internal reforming (IIR) approach, the reforming reactions appear in a reformer (within the cell) in close contact with the anode where the exothermic electrochemical reactions take place. The IR reactions decrease the requirement for cell cooling (less surplus of air). Less steam is needed and finally, it offers advantages with respect to the capital cost. Up to half of the heat produced by the oxidation reaction could be "consumed" by the steam reforming (SR) process. This would improve the system electrical efficiency [4,5].
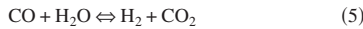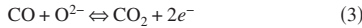
It is known that the use of heavy hydrocarbons ($C_4>$) can cause considerable coking and deactivation problems with SOFC anode catalysts. A prereformer can break down the hydrocarbons with longer coal chains to C_1 to C_2 molecules plus H_2 and CO [6]. An important part of the system design is the heat recovery, a big fraction of the heat generated in the cell can be used for the steam reforming reaction [7].

In this paper, a single intermediate temperature SOFC design, which uses externally reformed renewable fuels (prereformed methanol and ethanol and natural gas) is studied. The renewable fuels are compared with natural gas due to the large quantity of information available in open literature. It would be interesting to apply DIR as well; however, more experimental studies need to be performed to achieve reliable kinetic data for Ni/YSZ reforming of methanol and ethanol. The approach with IIR is not yet very well developed but it can be an interesting design in the future.

1.1 Electrochemical and Reforming Reactions. The global reactions that take place within a SOFC using hydrogen, carbon monoxide, and methane as fuel can be described as: oxygen is reduced in the cathode (Eq. (1)). The oxygen ions are transported through the electrolyte, but the electrons are prevented to pass through the electrolyte. The electrochemical reactions (Eqs. (2) and (3)) take place in the anodic three-phase boundary (TPB). Methane needs to be reformed (Eq. (4)) before the electrochemi-

cal reactions. Carbon monoxide can be oxidized in the electrochemical reaction (Eq. (3)) but can also react with water (Eq. (5)). The reactions described here are the overall ones, more detailed reaction mechanisms can be found in Ref. [8]. Note that methane is not participating in the electrochemical reactions at the anodic TPB, it is catalytically converted within the anode into carbon monoxide and hydrogen, which are used as fuels in the electrochemical reactions [9],

$$O_2 + 4e^- \Leftrightarrow 2O^{2-} \tag{1}$$

$$H_2 + O^{2-} \Leftrightarrow H_2O + 2e^- \tag{2}$$

$$CO + O^{2-} \Leftrightarrow CO_2 + 2e^- \tag{3}$$

$$CH_4 + H_2O \Leftrightarrow 3H_2 + CO \tag{4}$$

$$CO + H_2O \Leftrightarrow H_2 + CO_2 \tag{5}$$
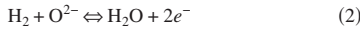
The net reaction of methanol, ethanol, and dimethyl ether (DME) to hydrogen and carbon monoxide are described in Eqs. (6)–(8), respectively. The produced carbon monoxide reacts then further with steam to hydrogen and carbon dioxide by the water-gas shift reaction, Eq. (5) [10],

$$CH_3OH \Leftrightarrow 2H_2 + CO \tag{6}$$

$$C_2H_5OH + H_2O \Leftrightarrow 4H_2 + 2CO \tag{7}$$

$$CH_3OCH_3 + H_2O \Leftrightarrow 4H_2 + 2CO \tag{8}$$
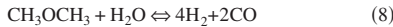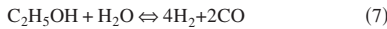
The steam reforming reaction rates for simple fuels is presented in Eqs. (4)–(8). Also more complex hydrocarbons (from renewable or fossil ori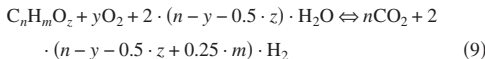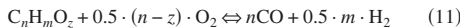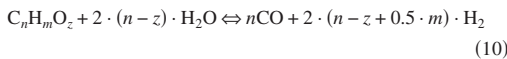gin) can be used as raw energy within a fuel cell system for hydrogen production. External reforming is necessary due to relatively long carbon chains. The overall hydrocarbon reforming reaction can be written as [7]

$$C_nH_mO_z + yO_2 + 2 \cdot (n - y - 0.5 \cdot z) \cdot H_2O \Leftrightarrow nCO_2 + 2$$
$$\cdot (n - y - 0.5 \cdot z + 0.25 \cdot m) \cdot H_2 \tag{9}$$

Equation (9) states the ideal reforming reaction where the only products are pure hydrogen and carbon dioxide. In reality within a fuel cell reformer, there are three ordinary reforming reactions: SR, partial oxidation (POX), and autothermal reforming (ATR). SR, Eq. (10), is effective for hydrogen production and largely exothermic. In POX, Eq. (11), the fuel is partially burned with a substoichiometric amount of air. An ATR system contains one reactor with SR and one with POX [7].

$$C_nH_mO_z + 2 \cdot (n - z) \cdot H_2O \Leftrightarrow nCO + 2 \cdot (n - z + 0.5 \cdot m) \cdot H_2 \tag{10}$$

$$C_nH_mO_z + 0.5 \cdot (n - z) \cdot O_2 \Leftrightarrow nCO + 0.5 \cdot m \cdot H_2 \tag{11}$$

It should be noted that if sufficient amount of heat is available, SR gives most hydrogen per amount of raw fuel; however, the conversion of complex hydrocarbons may be more difficult, compared with POX [7].

1.2 Renewable Fuels. Using alternative fuels (compared with hydrogen) gives SOFCs a major advantage because pure hydrogen is highly flammable and volatile, which makes it problematic to handle. Also, hydrogen has low density, which makes storing costly. It should also be mentioned that pure hydrogen is expensive to obtain since it has to be extracted from another source, most commonly natural gas [11].

Like hydrogen, methanol and ethanol are useful energy carriers rather than primary fuels (natural gas, coal, etc.) through gasification or chemical synthesis reforming processes. The characteristics of these alcohol-based fuels are very similar to conventional liquid fuels (propane, butane, and diesel) and can be readily handled, stored, and transported [10]. The CO_2 emissions do not

Table 1 Enthalpy change of reforming reaction for different fuels suitable for SOFCs [10]

Fuel	$\Sigma \Delta h_r$ (kJ/mol)	$\Sigma \Delta h_r / n_{H_2}$ (kJ/mol per mole of H_2 generated)
Methane	−165	−41.2
Methanol	−49.4	−16.5
DME	−121	−20.2
Ethanol	−173	−28.8

have to be an issue, when they are produced in a renewable manner, because it will lead to that the net effect on the emissions will be zero [12].

Methanol is interesting due to its ready availability, high specific energy, and easy storage and transportation. Ethanol is also a promising candidate since it is readily produced from renewable resources. When comparing these, ethanol has extra advantages in terms of power density, nontoxicity, transportation, and storage. However, because of incomplete oxidization, the ethanol processing reaction consists of a more complicated multistep reaction mechanism and involves a number of adsorbed intermediates and by-products. The chemical formula for biomass is generally written as $C_xH_yO_z$. The coefficients of x, y, and z can be calculated for each biomass. Biomass can be converted into biogas, usually by anaerobic breakdown in the absence of oxygen. The biogas consists mainly of methane and carbon dioxide [7].

Steam reforming of various fuels available in SOFCs, such as methane (biogas and natural gas), methanol, DME, and ethanol, consumes heat. The enthalpy change of the reaction for the mentioned fuels can be seen in Table 1. Ethanol consumes the most heat per mole of fuel. However, when considering that reforming of the different fuels generate a different amount of hydrogen (to be used in the electrochemical reactions), the most heat per mole of hydrogen generated is required by the reforming of methane. Globally, all the heat needed for the reforming reactions is generated within the cell, thanks to the electrochemical reactions, and a higher efficiency can be achieved with the mentioned renewable fuels compared with pure hydrogen. It should be mentioned that the temperature can decrease close to the inlet if the steam reforming reaction rate is too high.

1.3 Challenges With Renewable Fuels. The direct use of hydrocarbon fuels can lead to the catalyst's rapid deactivation by carbon formation on a traditional SOFC anode and also sulfur poisoning [13]. A high inlet temperature along with internal reforming of a hydrocarbon can cause a high temperature gradient and tensions within the anode close to the fuel inlet due to the fast steam reforming reaction rate. This problem can be reduced if the fuel inlet temperature is lowered, part of the anode gas is recycled, anode reforming activity is reduced, or if (partial) prereforming is employed [5].

The probability for carbon depositions depends on the steam-to-carbon ratio and operating temperature. It has been well established that the key reactions occur over a surface layer of nickel particles. If a layer of carbon is allowed to build up and attach to a nickel crystallite rapid catalyst breakdown can occur due to the graphite formation. It should be noted that hydrocarbons with a longer carbon chain than methane have a higher propensity for carbon deposition [5,14]. It is concluded that methane and methanol with appropriate steam content can be directly fed to Ni/YSZ anode without the problem of carbon formation [6]. For fuels with a longer carbon chain, a prereformer (with a catalyst less sensitive to carbon formation than Ni/YSZ) should be included in the fuel cell system.

Sulfur needs to be removed before the fuel enters into the cell to avoid degradation within the cell. Various methods can be applied, such as high temperature desulfurization, where organic sul-

Table 2 Cell geometry [2]

Cell component	Thickness
Cell length	0.1 m
Fuel channel height	1 mm
Air channel height	1 mm
Anode thickness	500 μm
Cathode thickness	50 μm
Electrolyte thickness	20 μm
Interconnect thickness	500 μm

fur compounds are reduced to hydrogen sulfite and the corresponding hydrocarbon, passing a cobalt or molybdenum catalyst supported on alumina. Adsorption methods can be applied for smaller SOFC systems [3].

For fuel cell systems, it is important to consider at what phase the fuel operates as the system can need extra equipments to handle the fuel storing and processing. The equipment besides the fuel cell generally takes up quite a lot of space and weight and for some fuels this becomes even more prominent when fuel storing space increases. Methane, DME, ammonia, and biogas are vapors at 1 bar and at 253–293 K. Methanol, ethanol, and diesel are liquids under these conditions. The vapors need to be pressurized to make the fuel storing in a commercial possible size with economically reasonable cost [15].

2 Mathematical Model

A two-dimensional model for an anode-supported SOFC is developed and implemented in the commercial software, COMSOL MULTIPHYSICS (version 3.5). Equations for momentum, mass, and heat transport are solved simultaneously. The geometry is defined in Table 2, and a sketch of the investigated cell can be seen in Fig. 1. Note the difference in scale between the cell length (x-direction, as in Fig. 1) and various component thicknesses (y-direction, as in Fig. 1). It should be mentioned that the model in this study is 2D only, and the connection between the electrodes and interconnect cannot be explicitly observed in this case.

2.1 Momentum Transport. The gases flow inside the fuel cell components, such as in the air and fuel channels, and in the porous electrodes. The Darcy–Brinkman equation is introduced and solved for the gas flow in the fuel and air channels and in the porous materials simultaneously [16,17]. The Darcy–Brinkman equation (Eq. (12)) is transformed into the standard Navier–Stokes equation when ($\kappa \rightarrow \infty$) and ($\varepsilon_p=1$) and into the Darcy equation as (Da$\rightarrow$0). Da is the Darcy number. The derivation of the Navier–Stokes and Darcy equations from the Darcy–Brinkman equation can be found in Ref. [16],

Fig. 1 Sketch of an anode-supported SOFC, not to scale

$$\left(\frac{\mu}{\kappa} + \rho \cdot \nabla \mathbf{u}\right)\mathbf{u} - \nabla\left[-p + \frac{1}{\varepsilon_p}\{\mathbf{T} - (\lambda)(\nabla \mathbf{u})\}\right] = \mathbf{F} \quad (12)$$

where $\mathbf{F}$ is the volume force vector, κ is the permeability of the porous medium, ε_p is the porosity, μ is the dynamic viscosity, $\mathbf{u}$ is the velocity vector, and $\mathbf{T}$ is the viscous stress tensor ($\mathbf{T}=v(\nabla \mathbf{u} +(\nabla \mathbf{u})^T)$). λ is the second viscosity; it is normally assumed as $\lambda=-2\mu/3$ [18]. The densities and viscosities for the participating gases are dependent on local concentration and temperature, as described in Refs. [2,11]. The gas inlet velocities are defined as a laminar flow profile. The outlet is defined as pressure (=1 atm).

2.2 Mass Transport. The Maxwell–Stefan equation for mass diffusion and convection is used to describe the mass transport phenomena for the gases inside the fuel cell [17]. The Maxwell–Stefan equation is solved for the fuel and air channels and the electrodes,

$$\nabla\left(-\rho \cdot w_i \sum^{n} \bar{D}_{ij} \cdot \nabla x_j(x_j - w_j)\frac{\nabla p}{p} \cdot \mathbf{u} - D_i^T \cdot \frac{\nabla T}{T}\right) + \rho \cdot \mathbf{u} \cdot \nabla w_j = S_i \quad (13)$$

where w is the mass fraction, x is the molar fraction, n is the number of species, D_i^T is the thermal diffusion coefficient, and D_{ij} is the Maxwell–Stefan binary diffusion coefficient. S_i, source term by chemical reactions, is only defined for the internal reforming reactions because the electrochemical reactions are assumed to take place at the interfaces between the electrolyte and electrodes. The diffusion coefficient is dependent on temperature, as described in Refs. [2,11]. On the air side, nitrogen and oxygen are involved, and only one Maxwell–Stefan diffusion coefficient needs to be calculated. On the fuel side, methane, water, hydrogen, carbon monoxide, and carbon dioxide are present, and ten pairs of Maxwell–Stefan diffusion coefficient need to be calculated. The boundary conditions for the mass transport equation are defined as mass fraction for the gas channel inlets; the outlets are defined as convective flux [2].

2.3 Heat Transport. The temperature distribution is calculated separately for the gas phase (in air and fuel channels and electrodes) and for the solid phase (interconnects, electrodes, and electrolyte). Heat is transferred between the phases at the channel walls and in the porous electrodes. The general heat conduction equation is used to calculate the temperature distribution for the solid materials, i.e., electrolyte, interconnect, and electrodes [17],

$$\nabla(-k_s \cdot \nabla T_s) = Q_s \quad (14)$$

where k_s is the thermal conductivity of the solids, T_s is the solid temperature, and Q_s is the heat source (heat transfer between the solid and gas phases and heat generation due to Ohmic polarization). Note that heat generated due to Ohmic polarization is assumed to enter the solid phase (as a part of Q_s), heat generation due to electrochemical reactions, concentration and activation polarization are simplified and defined as interface conditions, such as for the mass transport. The temperature distribution for the gas mixtures in the fuel and air channels and in the porous electrodes is calculated as [17]

$$\nabla(-k_g \cdot \nabla T_g) = Q_g - \rho_g \cdot c_{p,g} \cdot \mathbf{u} \cdot \nabla T_g \quad (15)$$

in which $c_{p,g}$ is the gas phase heat capacity, T_g is the temperature in the gas phase, and Q_g is the heat transfer between the gas and solid phases. Because the Reynolds number is small, the heat transfer coefficient ($h_{s,g,\text{por}}$) in the porous electrodes (spherical particles are assumed) can be calculated as [19]
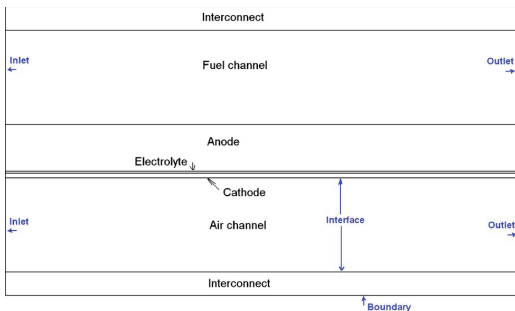
$$h_{s,g,\text{por}} = \frac{2 \cdot k_g}{d_p} \qquad (16)$$

where d_p is the electrode particle diameter and k_g is the gas conductivity. The heat transfer between the gas and solid phase depends on the temperature difference and the particle area to volume ratio as [20]

$$Q_g = h_v \cdot (T_g - T_s) = AV \cdot h_{s,g,\text{por}} \cdot (T_g - T_s) \qquad (17)$$

in which h_v is the volume heat transfer coefficient and AV is the area to volume ratio, which is used for heat transfer between the solid and gas phase. Note that the surface to volume ratio for heat transfer is higher than that for chemical reactions because not all the available surface is covered with active nickel catalyst. The heat transfer area to volume ratio equals to the material specific available area (area per weight) times the density. The heat capacity and the thermal conductivity in the gas phase depend on the temperature and the concentration, as described in Refs. [2,11]. The heating due to Ohmic polarization is described in Sec. 2.4.

The inlet gas temperature is defined by the operating temperature (1000 K), and the outlet one is defined as a convective flux. The boundaries at the top and at the bottom of the cell are defined by symmetries because it is assumed that the cell is surrounded by other cells with the same temperature distribution. The heat flux between the electrodes/interconnect and gas channels are specified at two channel walls, located opposite to each other, with a constant Nusselt number (4.094) from Ref. [21], based on the fully developed flow for a rectangular duct (aspect ratio is 1 for both channels). The cell is also heated due to change in entropy in the electrochemical reactions and concentration and activation polarizations, as described in Sec. 2.4.

2.4 Electrochemical Reactions. Two approaches for defining the electrochemical reactions can be found in literature, either as source terms in the governing equations [22,23] or as interface conditions defined at the electrode/electrolyte interfaces [24,25]. The later approach is employed in this study because the thickness of the active layer is sufficiently thin, compared with the thickness of the electrode [24,25]. The charge transfer equations are not solved in this study; however, the temperature effects from Ohmic, concentration, and activation polarization losses are included in the equations for heat transport.

Both hydrogen and carbon monoxide can participate in electrochemical reactions with oxygen ions (Eqs. (2) and (3)). The electrochemical oxidation of hydrogen is several times higher than that of carbon monoxide while the water-gas shift reaction is relatively fast [23]. The contribution of oxidation of carbon monoxide has been neglected in this study. The cell average current density in this study is specified as 0.3 A/cm^2.

Ohmic polarization occurs due to resistance of the flow of ions in the electrolyte and electrical resistance in the electrodes. The electrodes and electrolyte are heated due to this effect [26,27],

$$Q_{\text{ohm}} = \frac{i \cdot \eta_{\text{ohm}}}{\tau} \qquad (18)$$

$$\eta_{\text{ohm}} = R_{\text{ohm}} \cdot i \qquad (19)$$

$$R_{\text{ohm}} = \frac{\tau_a}{\sigma_a} + \frac{\tau_{\text{el}}}{\sigma_{\text{el}}} + \frac{\tau_c}{\sigma_c} \qquad (20)$$

where τ is the component thickness and R_{ohm} is the electrolyte area-specific Ohmic resistance. The electronic/ionic conductivities (σ) are calculated as described in Ref. [26].

Heat generated due to electrochemical reactions and due to polarization losses are, as previously described, defined at the electrodes/electrolyte interfaces,

$$- n \cdot (- k \nabla T) - = q_0 \qquad (21)$$

$$q_0 = q_r + q_{\text{losses}} = - i \cdot \left(\frac{T \cdot \Delta S_r}{n_e \cdot F} + \eta_{\text{act},e} + \eta_{\text{conc},e} \right) \qquad (22)$$

where q_0 is the heat generated at the interface (specified as interface condition), q_r is the heat generated inside the cell due to change in enthalpy, and q_{losses} is the heat generated due to potential losses inside the cell. The amount of heat generated due to electrochemical reactions can be calculated as [28]

$$q_r = - T \cdot \Delta S_r \cdot \dot{n} = - \Delta S_r \frac{T \cdot i}{n_e F} \qquad (23)$$

$$\dot{n} = \frac{i}{n_e F} \qquad (24)$$

where $\dot{n}$ is the molar flux density (mol/(m^2 s)) and ΔS_r is entropy change of reaction (-50.2 J/(K mol)), calculated from data in Ref. [29]. The heat generation due to activation and concentration polarizations can be calculated as [27,30]

$$q_{\text{losses}} = - i \cdot (\eta_{\text{act},e} + \eta_{\text{conc},e}) \qquad (25)$$

The concentration polarizations due to concentration differences inside the cell are specified as [26]

$$\eta_{\text{conc},a} = \frac{RT}{n_{e,a}F} \ln \left(\frac{p_{\text{H}_2\text{O,TPB}} \cdot p_{\text{H}_2,b}}{p_{\text{H}_2,\text{TPB}} \cdot p_{\text{H}_2\text{O},b}} \right) \qquad (26)$$

$$\eta_{\text{conc},c} = \frac{RT}{n_{e,c}F} \ln \left(\frac{p_{\text{O}_2,b}}{p_{\text{O}_2,\text{TPB}}} \right) \qquad (27)$$

where $p_{i,\text{TPB}}$ stands for the partial pressure at the boundary TPB and $p_{i,b}$ is the partial pressure at the interface between gas channel and electrode. Chemical reactions involve energy barriers (i.e., activation polarization), which must be overcome by the reacting species. The activation polarization can be considered as the extra potential needed to overcome the energy barrier of the rate-determining step to a value that the reaction proceeds at a desired rate [30],

$$\eta_{\text{act},e} = \frac{2RT}{n_e F} \sinh^{-1} \left(\frac{i_e}{2 \cdot i_{0,e}} \right) \qquad (28)$$

$$i_{0,e} = \frac{RT}{n_e F} k''_e \exp \left(\frac{-E_e}{RT} \right) \qquad (29)$$

where $i_{0,e}$ is the exchange current density. The pre-exponential factor (k'') is 2.35×10^{11} Ω^{-1} m^{-2} for the cathode and 6.54×10^{11} Ω^{-1} m^{-2} for the anode, respectively. The activation energy (E) is 137 kJ/mol for the cathode and 140 kJ/mol for the anode [26].

2.5 Internal Reforming Reactions. Sufficient activity for the reforming reactions is provided inside the SOFC anode [31]. Reaction kinetics from Ref. [32] for the steam reforming (an expression dependent on the active area to volume ratio) and from Ref. [33] for the water-gas shift reactions are used to calculate the reaction rates in this work. Other global kinetic models can be found in Refs. [34,35]. The catalytic steam reforming reaction occurs at the surface of the nickel catalyst and is specified as [32,36]

$$r_r = AV \cdot \left(943 \exp \left(\frac{-225 \times 10^3}{R \cdot T} \right) \cdot p_{\text{CH}_4} p_{\text{H}_2\text{O}} \right.$$
$$\left. - 7.74 \times 10^{-9} \exp \left(\frac{-1937}{R \cdot T} \right) \cdot p_{\text{CO}} p_{\text{H}_2}^3 \right) \qquad (30)$$

where p_i is the partial pressure of gas species i, T is the temperature, r is the reaction rate, and AV is the active area to volume ratio. Equation (30) originates from experiments performed at the Research Center Jülish, and the anode material consists of Ni-

8YSZ substrate with a standard composition of $C_nH_mO_z$ Ni [36].

The range for the AV (related to catalytic kinetic reactions) varies in literature between 1×10^5 m^2/m^3 [37] and 2.2 $\times 10^6$ m^2/m^3 [32] for SOFC anodes. The measured specific surface area (m^2/g) for Ni/YSZ material developed for SOFC anodes (with a pore size of 225 nm) is 70×10^6 m^2/m^3 [38]. Note that not all the surfaces are available for catalytic reactions due to the distribution of catalyst, nonavailable pores, and mass transfer limitations among others. An AV of 2.2×10^6 m^2/m^3, corresponding to 3.1% of the total Ni/YSZ specific area to volume ratio, is used in this work. The trend for the development during the past years is in the direction of employing smaller particles to get larger AV.

The reaction rate (Eq. (30)) is of the Arrhenius type. It consists of three parts, partial pressures, pre-exponential factor, and activation energy. The pre-exponential factor describes the amount of collisions between the molecules within the reaction and the exponential expression with the activation energy describes the probability for the reaction to occur. The pre-exponential factors depend strongly on the properties of the anode material and the temperature. The activation energy is based on the catalytic characteristics, such as chemical composition. The large difference between the activation energies in open literature [11,32,34–36,39] makes it probable that more parameters have significant influences on the reaction rate. To truly enhance the understanding of these phenomena, microscale modeling is needed.

Different approaches for defining the water-gas shift reaction can be found in literature: (1) global reaction mechanism that considers reaction in the anode only [9,23,33], (2) global reaction mechanism that considers reaction in the anode and in the fuel channel [32,40], and (3) a more advanced reaction mechanism that includes catalytic surface reaction kinetics for integrated steam reforming, water-gas shift reaction, and the Boudouard mechanism [8,41]. Based on the global scheme for the anode, the expression for the catalyzed water-gas shift reaction in Ref. [33] has been selected in this study:

$$r_s = k_{sf} \cdot \left(p_{H_2O} p_{CO} - \frac{p_{H_2} p_{CO_2}}{K_{ps}} \right) \quad (31)$$

The rate constant (k_{sf}) and the equilibrium constant (K_{ps}) are temperature dependent expressions calculated from experimental data, as described in Ref. [33].

The source terms S_i (implemented in the Maxwell Stefan equation for mass transport), due to the catalytical reforming reactions, are defined as [23]

$$S_{H_2} = (3r_r + r_s) \cdot M_{H_2} \quad (32)$$

$$S_{CH_4} = -r_r \cdot M_{CH_4} \quad (33)$$

$$S_{H_2O} = (-r_r - r_s) \cdot M_{H_2O} \quad (34)$$

$$S_{CO} = (r_r - r_s) \cdot M_{CO} \quad (35)$$

where M_i is the molecular weight and S_i is the source term of species i. The last species (CO_2) can be obtained because the sum of the mass fractions equals unity. The heat generation/consumption due to the reforming reactions is specified in [11]

$$Q_s = \sum_i r_i \cdot \Delta h_i \quad (36)$$

where Δh_i is the enthalpy change due to the reactions and Q_s is the heat generation in the solid phase.

2.6 Cell Operating Conditions. The investigation performed in this study concerns biogas, preformed methanol, ethanol, and natural gas. The inlet molar fractions are specified in Table 3. The molar fractions based on initial steam-to-fuel ratios (SFs) of 3 and

Table 3 Inlet molar fractions

|	H_2	CO	CO_2	CH_4	H_2O
Methanol, SF=3	0.270	0.115	0.051	0.017	0.547
Methanol, SF=5	0.247	0.072	0.042	0.011	0.628
Ethanol, SF=3	0.359	0.114	0.030	0.112	0.385
Ethanol, SF=5	0.312	0.081	0.036	0.080	0.491
Biogas steam mixture	0.03	0	0.27	0.36	0.34
30% preformed natural gas [11]	0.263	0.0294	0.0436	0.171	0.493

5 (for methanol and ethanol) are calculated from the experiments performed in Ref. [6]. After the prereforming of ethanol, the fuel mixture contains some ethylene and etan. To simplify the calculation and due to the lack of kinetic information in considering reforming of ethylene and etan on Ni/YSZ catalyst, these concentrations are assumed to be methane. For the case of biogas, a small fraction of hydrogen is added to enable electrochemical reactions close to the inlet as well, and steam is added to avoid carbon deposition and to be used in the reforming reactions. The fuel composition for 30% preformed natural gas is defined by the International Energy Agency (IEA) and is frequently used in literature. The flow rates for the different cases are calculated to keep the fuel utilization being 80%. The flow rate of air is kept constant for all cases and the oxygen utilization is set to be 20%.

3 Results and Discussion

The predicted temperature distribution for the case with preformed methanol with initial SFs of 3 and 5 can be seen in Figs. 2 and 3, respectively. Increased SF means a slightly decreased temperature rise (5 K difference in the maximum temperature between these two cases) due to a higher flow rate in the flow channel (to keep the fuel utilization to 80%). It should be mentioned that the flow rate in the air channel is significantly higher than in the fuel channel. The temperature difference in the y-direction (Fig. 4) in the air channels occurs because the convective heat flux are bigger in the air channel (compared with the fuel channel) due to the relatively larger air flow rate.

The temperature distribution for biogas is shown in Fig. 5, that for prereformed ethanol (SF=3) is shown in Fig. 6, and that for 30% prereformed natural gas is shown in Fig. 7. The case with biogas and natural gas contains more methane compared with that of prereformed ethanol and methanol. A higher fraction of methane means a decreased total temperature rise due to the heat consumption in the steam reforming reaction.

The developed model is also used to simulate cases with an even higher concentration of methane and also a higher inlet temperature (compared with the cases in Table 3). The limitation to be
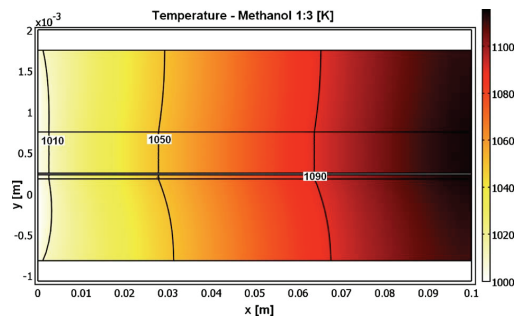
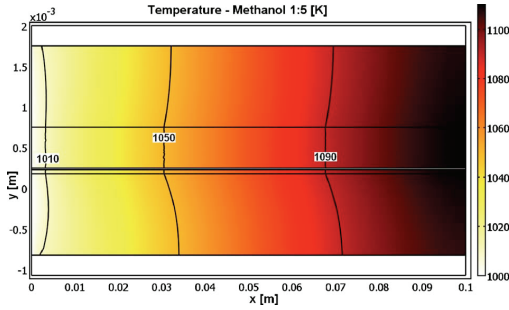**Fig. 2 Gas phase temperature distribution for prereformed methanol (SF=3)**

Fig. 3 Gas phase temperature distribution for prereformed methanol (SF=5)
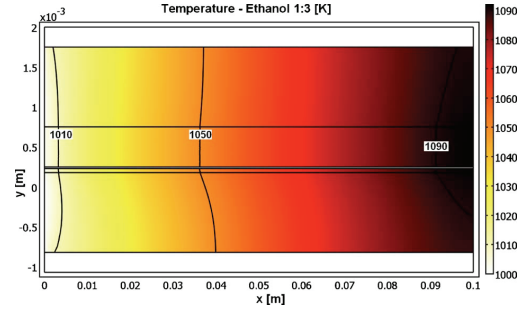

Fig. 6 Gas phase temperature distribution for prereformed ethanol (SF=3)

considered is that the probability of carbon deposition increases when the SC is too low. The potential trouble with a high temperature gradient close to the fuel inlet can be managed with lowering the inlet temperature or diluting the fuel since a higher temperature or a less diluted fuel gives a higher steam reforming reaction rate and also a higher temperature gradient. This is not a problem, for the cases specified in Table 3, since a relatively low inlet temperature (1000 K) as well as prereformed fuel mixtures is used. The activation energy in the methane steam reforming reaction is high for this case; i.e., the probability for reaction is very low. A catalytic composition with decreased activation energy will cause a steeper temperature gradient. When the inlet temperature is increased, a high temperature gradient close to the inlet can

occur, as observed in Fig. 8, where the inlet gas temperature for the case with biogas is increased with 100 K. Note that the heat generated by the electrochemical reactions and polarization losses is still higher than the heat consumed by the reforming reactions when the complete cell is studied.

The predicted molar fractions in the fuel channel for the participating gas species along the flow direction for the case with prereformed methanol (SF=3) are shown in Fig. 9, and those for the case with biogas are shown in Fig. 10. Hydrogen is consumed and water is generated (due to the electrochemical reactions) along the flow direction for all the investigated situations. There is a consumption of water as carbon monoxide and methane are reformed. Depending on the inlet fraction, a decrease in the molar fraction of water can be observed close to the inlet, e.g., for the
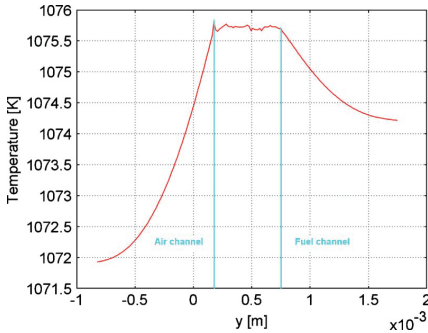

Fig. 4 Gas phase temperature distribution for prereformed methanol (SF=3) in the middle of the cell (at x=0.05 m)
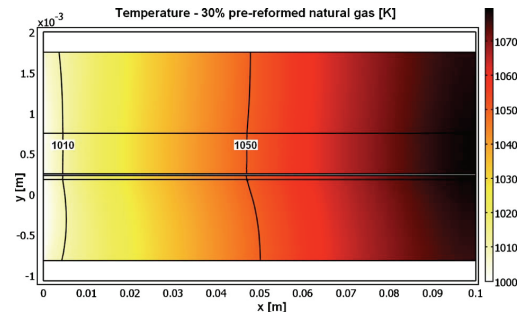

Fig. 7 Gas phase temperature distribution for 30% prereformed natural gas
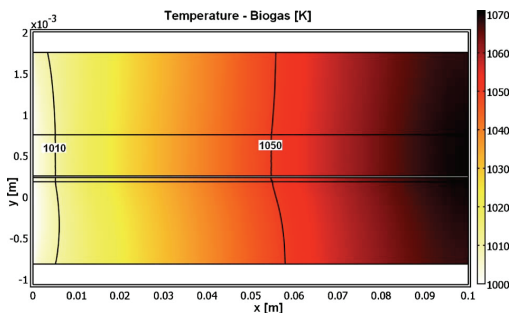

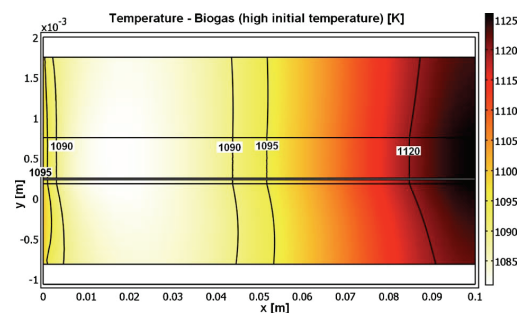**Fig. 5 Gas phase temperature distribution for biogas-steam mixture**

Fig. 8 Gas phase temperature distribution for biogas-steam mixture with an increased inlet temperature
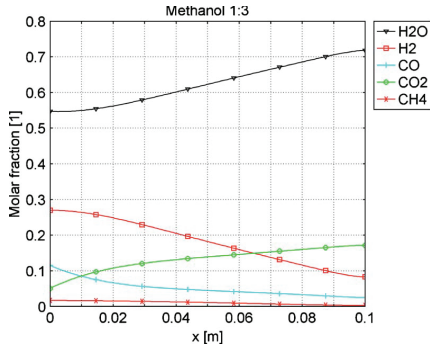
Fig. 9 Molar fraction of the gas species in the fuel channel along the flow direction for prereformed methanol (SF=3)

Fig. 11 Reaction rate (in mol/(m³ s)) for the steam reforming reaction within the anode for the case with biogas-steam mixture

cases with prereformed methanol. The molar fraction of carbon monoxide depends on the water-gas shift reaction. The case with biogas contains initially very little hydrogen. The generation of more hydrogen depends on the steam reforming reaction, which depends on the active area to volume ratio, temperature, and gas species concentrations. Note that the total amount of molecules (within the fuel cell) increases as the steam reforming reaction proceeds to the right.

For the situations with high inlet concentrations of methane (for example, the case with biogas, shown in Fig. 11), the steam reforming reaction rate (within the anode) is high as long as high concentration of methane is available. The lower rate close to the inlet is due to a lower temperature. The reaction rate expression has, as previously mentioned, high activation energy. This is the reason for the relatively low reaction rate, which enables the methane steam reforming reaction rate to be similar within the entire length of the anode. It should be mentioned that the backward reaction rate is negligible, compared with the forward reaction rate for the situations applied in this study. The reaction rate increases as the temperature and concentration of steam increase and decreases as the concentration of methane decreases. Note that there is a difference in scale between the x- and y-directions. The steam reforming reaction rate in the anode for the case with prereformed methanol (SF=3) is shown in Fig. 12. It contains initially very little methane. This gives a low initial steam reforming reaction rate, which increases as the carbon monoxide and the hydrogen are consumed, as well as the temperature is increased. It
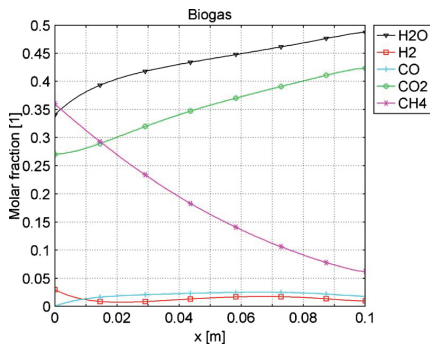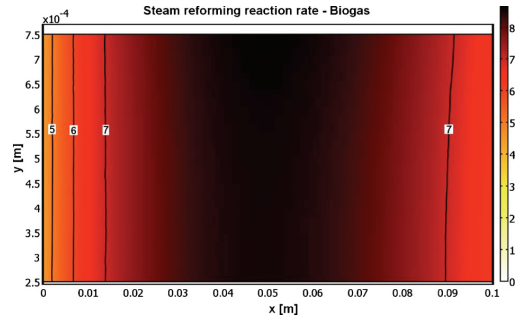
is possible to change the reaction rate, either by changing the particle size of active catalyst or the porous structure, i.e., active catalytic area.

As shown in Fig. 13, high reaction rates for the water-gas shift reaction are obtained when the inlet concentrations are far from equilibrium conditions in terms of temperature and concentrations, for example, for methanol with the SF of 3. The reaction rate for the water-gas shift reaction in the anode for the case with biogas is shown in Fig. 14. The reaction proceeds initially to the left due to a low concentration of carbon monoxide and a high concentration of carbon dioxide. As hydrogen is consumed and water generated by the electrochemical reaction within the anode, this reaction proceeds to the right. The water-gas shift reaction is
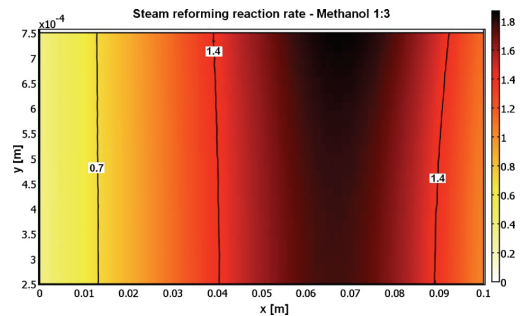
Fig. 12 Reaction rate (in mol/(m³ s)) for the steam reforming reaction within the anode for prereformed methanol (SF=3)
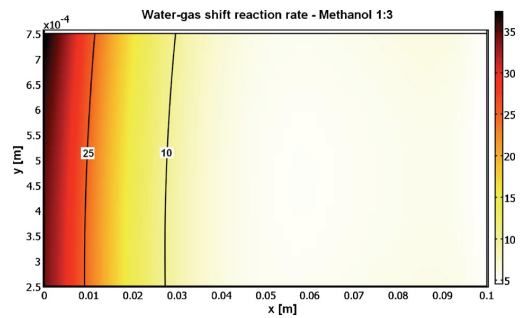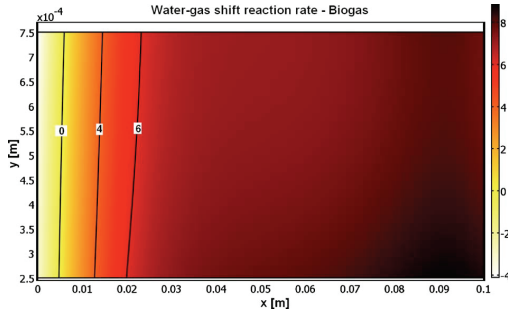

Fig. 13 Reaction rate (in mol/(m³ s)) for the water-gas shift reaction within the anode for prereformed methanol (SF=3)

Fig. 10 Molar fraction of the gas species in the fuel channel along the flow direction for biogas-steam mixture

Journal of Fuel Cell Science and Technology

JUNE 2011, Vol. 8 / **031013-7**

Fig. 14 Reaction rate (in mol/(m³ s)) for the water-gas shift reforming reaction within the anode for biogas-steam mixture

coupled to the steam reforming reaction, due to the production of carbon monoxide and hydrogen, and consumption of water.

No validation with experimental data has been conducted. However, some comparison with literature has been done. The result in this study follows the same trend concerning temperature and concentration distributions along the flow direction as in Refs. [32,40,41].

4 Conclusions

A CFD approach is developed and implemented to analyze physical phenomena, which take place inside a single anode-supported SOFC. Equations for mass, heat, and momentum transport are solved simultaneously. The temperature distributions in the gas and solid phases are calculated separately according to the local temperature nonequilibrium approach. The operating parameters are kept constant, while the inlet fuel compositions are varied to illustrate biogas, preformed methanol, ethanol, and natural gas.

The heat, which is generated due to the electrochemical reactions, can be used for internal steam reforming reaction within the anode and/or outside the cell for external reforming and preheating of the fuel and air. It is concluded that a fuel containing a high percentage of methane and also a high inlet temperature gives a steep temperature gradient close to the fuel inlet (i.e., the case with biogas and an increased inlet temperature). The case with preformed methanol contains only a small amount of methane, which makes the total heat generation higher, compared with the other investigated cases. It is found that for the steam reforming reaction, the backward reaction rate is negligible, compared with the forward one, for the conditions within a SOFC. The probability for methane steam reforming reaction is low due to the high activation energy. To increase the reaction rate significantly, a new catalytic composition should be introduced. The low reforming reaction rate has advantages in terms of a low temperature gradient, i.e., decreased risk of mechanical failure.

It is concluded that biogas, methanol, and ethanol are suitable alternative fuels for a SOFC system. The reforming of ethanol is more complex and gives more by-products compared with the reforming of methanol and methane. Utilization of a fuel with an even longer coal chain makes the reforming more complex and the possibility of internal reforming (within the anode) disappear. Addition of more steam to fuel decreases the risk of carbon deposition at the anode catalytic active area.

Further development of SOFCs can enhance the transition from fossil fuels to renewable fuels. The choice of the fuel for a commercial fuel cell system will depend on the available fuel infrastructure, complexity of system, environmental requirements to be considered, and price for the different fuels.

Nomenclature

AV = (active) area to volume ratio, m²/m³
c_p = specific heat capacity at constant pressure, J/kg K
Da = Darcy number, dimensionless
D_{ij} = Maxwell–Stefan binary diffusion coefficient, m²/s
D_i^T = thermal diffusion coefficient, kg/(m s)
d_p = electrode particle diameter, m
E = activation energy, kJ/mol
$\mathbf{F}$ = volume force vector, N/m³
F = Faraday constant, 96,485 C/mol
h = enthalpy, J/mol
$h_{s,g}$ = heat transfer coefficient, W/(m² K)
h_v = volume heat transfer coefficient, W/(m³ K)
i = current density, A/cm²
i_0 = exchange current density, A/cm²
k = thermal conductivity, W/m/K
k'' = pre-exponential factor, 1/(Ω m²)
M_j = molar mass of species j, kg/mol
n_e = number of electrons transferred per reaction
p_i = pressure of species i, Pa
q = heat flux, W/m²
Q = source term (heat), W/m³
R = gas constant, 8.314 J/mol K
r = reaction rate, mol/(m² s), mol/(m³ s)
R_{ohm} = electrolyte area-specific Ohmic resistance, Ω/m²
S_i = source term (mass), kg/(m³ s)
$\mathbf{T}$ = viscous stress tensor, N/m
T = temperature, K
u = velocity field, m/s
v = dynamic viscosity, Pa s
w_i = mass fraction of species i, kg/kg
x, y = coordinate system, m
x_j = molar fraction of species j, mol/mol
ΔS_r = entropy of reaction, J/K mol

Greek Symbols

ε_p = porosity, dimensionless
η = over potential, V
κ = permeability, m²
λ = second viscosity, Pa s
μ = dynamic viscosity, Pa s
ρ = density, kg/m³
σ = ionic/electronic conductivity, Ω⁻¹ m⁻¹
τ = component thickness, m

Subscripts

0 = initial
a = anode
act = activation polarization
c = cathode
conc = concentration polarization
e = electrode, $e \in \{a, c\}$
el = electrolyte
g = gas phase
i = molecule i
j = molecule j
losses = activation and concentration polarization
ohm = Ohmic polarization
por = porous media
r = steam reforming reaction

s = solid phase, water-gas shift reaction

Chemical

C_2H_5OH = ethanol
CH_3OCH_3 = dimethyl ether (DME)
CH_3OH = methanol
CH_4 = methane
$C_nH_mO_z$ = hydrocarbon with a carbon chain of n atoms
CO = carbon monoxide
CO_2 = carbon dioxide
e^- = electron
H_2 = hydrogen
H_2O = water
Ni = nickel
O_2 = oxygen
YSZ = yttria-stabilized zirconia

References

[1] Staniforth, J., and Ormerod, M., 2002, "Implications for Using Biogas as a Fuel Source for Solid Oxide Fuel Cells: Internal Dry Reforming in a Small Tubular Solid Oxide Fuel Cell," Catal. Lett., **81**, pp. 19–23.

[2] Andersson, M., Yuan, J., Sundén, B., and Wang, W. G., 2009, "LTNE Approach and Simulation for Anode-Supported SOFCs," *Proceedings of the Seventh International Fuel Cell Science, Engineering and Technology Conference*, Newport Beach, CA.

[3] Ormerod, R. M., 2004, "Fuels and Fuel Processing in Solid Oxide Fuel Cells," *Solid Oxide Fuel Cells*, S. C. Singhal and K. Kendall, eds., Springer-Verlag, Berlin, pp. 333–362.

[4] Dokmaingam, P., Assabumrungrat, S., Soottitantawat, A., and Laosiripojana, N., 2010, "Modelling of Tubular-Designed Solid Oxide Fuel Cell With Indirect Internal Reforming Operation Fed by Different Primary Fuels," J. Power Sources, **195**, pp. 69–78.

[5] Andersson, M., Paradis, H., Yuan, J., and Sundén, B., 2010, "Catalyst Materials and Catalytic Steam Reforming Reactions in SOFC Anodes," *Proceedings of the International Green Energy Conference*, Waterloo, ON, Canada.

[6] Laosiripojana, N., and Assabumrungrat, S., 2007, "Catalytic Steam Reforming of Methane, Methanol and Ethanol Over Ni/YSZ: The Possible Use of These Fuels in Internal Reforming SOFC," J. Power Sources, **163**, pp. 943–951.

[7] Xuan, J., Leung, M. K. H., Leung, D. Y. C., and Ni, M., 2009, "A Review of Biomass-Derived Fuel Processors for Fuel Cell Systems," Renewable Sustainable Energy Rev., **13**, pp. 1301–1313.

[8] Janardhanan, V., and Deutschmann, O., 2006, "CFD Analysis of a Solid Oxide Fuel Cell With Internal Reforming," J. Power Sources, **162**, pp. 1192–1202.

[9] Ni, M., Leung, M. K. H., and Leung, D. Y. C., 2007, "Micro-Scale Modeling of Solid Oxide Fuel Cells With Micro-Structurally Grades Electrodes," J. Power Sources, **168**, pp. 369–378.

[10] Cocco, D., and Tola, V., 2009, "Use of Alternative Hydrogen Energy Carriers in SOFC-MGT Hybrid Power Plants," Energy Convers. Manage., **50**, pp. 1040–1048.

[11] Andersson, M., 2009, "SOFC Modeling Considering Mass and Heat Transfer, Fluid Flow With Internal Reforming Reactions," Licentiate thesis, Department of Energy Sciences, Lund University, Sweden.

[12] Mignard, D., and Pritchard, C., 2008, "On the Use of Electrolytic Hydrogen From Variable Renewable Energies for the Enhanced Conversion of Biomass to Fuels," Chem. Eng. Res. Des., **86**, pp. 473–487.

[13] Cimenti, M., and Hill, J. M., 2009, "Thermodynamic Analysis of Solid Oxide Fuel Cells Operated With Methanol and Ethanol Under Direct Utilization, Steam Reforming, Dry Reforming or Partial Oxidation Conditions," J. Power Sources, **186**, pp. 377–384.

[14] Clarke, S., Dicks, A., Pointon, K., Smith, T., and Swann, A., 1997, "Catalytic Aspects of the Steam Reforming of Hydrocarbons in Internal Reforming Fuel Cells," Catal. Today, **38**, pp. 411–423.

[15] Paradis, H., Andersson, M., Yuan, J., and Sundén, B., 2010, "Review of Different Renewable Fuels for Potential Utilization in SOFCs," *Proceedings of the International Green Energy Conference*, Waterloo, ON, Canada.

[16] Le Bars, M., and Worster, M. G., 2006, "Interfacial Conditions Between a Pure Fluid and a Porous Medium, Implications for Binary Alloy Solidification," J. Fluid Mech., **550**, pp. 149–173.

[17] COMSOL, 2008, COMSOL MULTIPHYSICS 3.5 User Guide, Stockholm, Sweden.

[18] Versteeg, H. K., and Malalasekera, W., 1995, *An Introduction to Computational Fluid Dynamics, The Finite Volume Method*, Pearson, UK.

[19] Damm, D. L., and Fedorov, A. G., 2006, "Local Thermal Non-Equlibrium Effects in Porous Electrodes of the Hydrogen Fueled SOFC," J. Power Sources, **159**, pp. 1153–1157.

[20] Chao, C. H., and Hwang, A. J. J., 2006, "Predictions of Phase Temperatures in a Porous Cathode of Polymer Electrolyte Fuel Cells Using a Two-Equation Model," J. Power Sources, **160**, pp. 1122–1130.

[21] Shah, R. K., and London, A. L., 1978, *Laminar Flow Forced Convection in Ducts*, Academic, London, UK.

[22] Hussain, M. M., Li, X., and Dincer, I., 2007, "Mathematical Modeling of Transport Phenomena in Porous SOFC Anodes," Int. J. Therm. Sci., **46**, pp. 48–56.

[23] Yuan, J., Huang, Y., Sundén, B., and Wang, W. G., 2009, "Analysis of Parameter Effects on Chemical Coupled Transport Phenomena in SOFC Anodes," Heat Mass Transfer, **45**, pp. 471–484.

[24] Suwanwarangkul, R., Croiset, E., Fowler, M. W., Douglas, P. L., Entchev, E., and Douglas, M. A., 2003, "Dusty-Gas and Stefan-Maxwell Models to Predict the Concentration Overpotential of a SOFC Anode," J. Power Sources, **122**, pp. 9–18.

[25] Tseronis, K., Kookos, I. K., and Theodoropoulos, C., 2006, "Modeling Mass Transport in Solid Oxide Fuel Cell Anodes: A Case for a Multidimensional Dusty Gas-Based Model," Chem. Eng. Sci., **63**, pp. 5626–5638.

[26] Patcharavorachot, Y., Arpornwichanop, A., and Chuachuebsuk, A., 2008, "Electrochemical Study of a Planar Solid Oxide Fuel Cell: Role of Support Structures," J. Power Sources, **177**, pp. 254–261.

[27] Chan, S. H., Low, C. F., and Ding, O. L., 2002, "Energy and Exergy Analysis of Simple Solid-Oxide Fuel-Cell Power Systems," J. Power Sources, **103**, pp. 188–200.

[28] Bove, R., and Ubertini, S., 2006, "Modeling Solid Oxide Fuel Cell Operation: Approaches, Techniques and Results," J. Power Sources, **159**, pp. 543–559.

[29] Bessler, W. G., Warnatz, J., and Goodwin, D. G., 2007, "The Influence of Equilibrium Potential on the Hydrogen Oxidation Kinetics of SOFC Anodes," Solid State Ionics, **177**, pp. 3371–3383.

[30] Chan, S. H., Khor, K. A., and Xia, Z. T., 2001, "A Complete Polarization Model of a Solid Oxide Fuel Cell and Its Sensitivity to Change of Cell Component Thickness," J. Power Sources, **93**, pp. 130–140.

[31] Ferguson, J. R., Fiard, J. M., and Herbin, R., 1996, "Three-Dimensional Numerical Simulation for Various Geometries of Solid Oxide Fuel Cells," J. Power Sources, **58**, pp. 109–122.

[32] Klein, J.-M., Bultel, Y., Georges, S., and Pons, M., 2007, "Modeling of a SOFC Fuelled by Methane: From Direct Internal Reforming to Gradual Internal Reforming," Chem. Eng. Sci., **62**, pp. 1636–1649.

[33] Haberman, B. A., and Young, J. B., 2004, "Three-Dimensional Simulation of Chemically Reacting Gas Flows in the Porous Support Structure of an Integrated-Planar Solid Oxide Fuel Cell," Int. J. Heat Mass Transfer, **47**, pp. 3617–3629.

[34] Nagel, F., Schildhauer, T., Biollaz, S., and Stucki, S., 2008, "Charge, Mass and Heat Transfer Interactions in Solid Oxide Fuel Cells Operated With Different Fuel Gases—A Sensitivity Analysis," J. Power Sources, **184**, pp. 129–142.

[35] Sanchez, D., Chacartegui, R., Munoz, A., and Sanchez, T., 2008, "On the Effect of Methane Internal Reforming in Solid Oxide Fuel Cells," Int. J. Hydrogen Energy, **33**, pp. 1834–1844.

[36] Drescher, I., Lehnert, W., and Meusinger, J., 1998, "Structural Properties of SOFC Anodes and Reactivity," Electrochim. Acta, **43**(19–20), pp. 3059–3068.

[37] Danilov, V., and Tade, M., 2009, "A CFD-Based Model of a Planar SOFC for Anode Flow Field Design," Int. J. Hydrogen Energy, **34**, pp. 8998–9006.

[38] Marrero-López, D., Ruiz-Morales, J. C., Peña-Martínez, J., Canales-Vázquez, J., and Núñez, P., 2008, "Preparation of Thin Layer Material With Macroporous Microstructure for SOFC Applications," J. Solid State Chem., **181**, pp. 685–692.

[39] Paradis, H., Andersson, M., Yuan, J., and Sundén, B., 2010, "CFD Modeling Considering Different Kinetic Models for Internal Reforming Reactions in an Anode-Supported SOFC," *Proceedings of the Eighth International Fuel Cell Science, Engineering and Technology Conference*, Brooklyn, NY.

[40] Aguiar, P., Adjiman, C. S., and Brandon, N. P., 2004, "Anode-Supported Intermediate Temperature Direct Internal Reforming Solid Oxide Fuel Cell. I: Model-Based Steady-State Performance," J. Power Sources, **138**, pp. 120–136.

[41] Hofmann, P., Panopoulos, K. D., Fryda, L. E., and Kakaras, E., 2009, "Comparison Between Two Methane Reforming Models Applied to a Quasi-Two-Dimensional Planar Solid Oxide Fuel Cell Model," Energy, **34**, pp. 2151–2157.